Desalination and Water Treatment
www.deswater.com
doi: 10.1080/19443994.2015.1048306

57 (2016) 11956–11971
June

Taylor & Francis
Taylor & Francis Group

Mathematical and CFD modeling of vacuum membrane distillation for desalination

Sushant Upadhyaya, Kailash Singh*, S.P. Chaurasia, Rajeev Kumar Dohare, Madhu Agarwal

Department of Chemical Engineering, Malaviya National Institute of Technology Jaipur, J.L.N. Marg, Jaipur, India, Tel. +91 141 2713486; email: supadhyay.chem@mnit.ac.in (S. Upadhyaya), Tel. +91 141 2713392; email: ksingh.mnit@gmail.com (K. Singh), Tel. +91 141 2713339; email: spchaurasia.chem@mnit.ac.in (S.P. Chaurasia), Tel. +91 141 2713485; email: rkdohare.chem@mnit.ac.in (R.K. Dohare), Tel. +91 141 2713498; email: magarwal.chem@mnit.ac.in (M. Agarwal)

Received 1 November 2014; Accepted 24 April 2015

ABSTRACT

In this work, a mathematical model has been developed for vacuum membrane distillation incorporating molecular diffusion–Knudsen diffusion–Poiseuille flow and validated with the experimental data. The feed-side membrane surface temperature used in mathematical model was estimated by computational fluid dynamics modeling. The effects of different operating parameters such as feed flow rate, feed bulk temperature, inlet concentration, and permeate-side pressure on water flux and salt rejection have been studied using PTFE membrane. It has been shown that with variation in feed flow rate from 0.5 to 2 lpm, the permeate flux increased from 20.1 to 25.6 kg/m^2 h. Similarly, with increase in feed bulk temperature from 40 to 60°C, the permeate flux increased from 2.10 to 26.6 kg/m^2 h. The permeate flux showed the variation from 17.8 to 19.5 kg/m^2 h on decreasing permeate pressure from 7 to 5.5 kPa. No significant effect of feed salt concentration was observed on permeate flux. More than 99% rejection was obtained at the feed salt concentration of 40,000 ppm of NaCl. Few runs were also carried out by taking multi-ion feed (Ca^{++}, Mg^{++}, Na^+, K^+, Cl^-, SO_4^{--}, Fe^{++}, NO_3^-, F^-) equivalent to that in ground water; in which case also more than 99% rejection was obtained.

Keywords: Mathematical modeling; CFD; Vacuum membrane distillation; Desalination; PTFE

1. Introduction

Desalination technologies have been known as the primary method of producing abundant water supplies, and the usage as well as efficiency of desalination technologies originates at a rate of about 4% per year (US Bureau of Reclamation and Sandia National Laboratories, 2003). Due to this reason, industries have applied the concept of desalination in order to produce fresh and safe water from saline water. Various technologies are available for desalination and purification of saline water such as membrane technologies, thermal technologies, and reuse/recycling technologies. The basis of all technologies is the conversion of part of the feed water into permeate or fresh water. Nevertheless, it must be understood that any desalination and water purification technology

*Corresponding author.

creates two output streams, viz a permeate (product) stream and a brine or concentrate (retentate) stream.

Many techniques have been investigated for the desalination of water and separation of salts. The most commonly used is reverse osmosis although other techniques such as thermal desalination and evaporation have been investigated [1]. The main shortcoming of reverse osmosis is the need for excessively high pressures at high solute concentration, as in the case of high saline industrial water such as ash and mine water [2]. An elevated pressure is required in order to overcome the osmotic pressure barrier in concentrate processing. In processes such as thermal evaporation, high temperatures are required in order to achieve evaporation and salt recovery.

Membrane distillation (MD) is one of the emerging non-isothermal membrane separation processes known for about 50 years. MD is a technique which leads to an almost complete water recovery. MD defined as thermally driven transport process of vapor through hydrophobic membranes, the basic driving force involved in MD is the vapor pressure difference between both sides of membrane. But, in other membrane separation processes, the basic driving force is the chemical potential difference through the membrane thickness [3–5]. Different MD configurations such as direct contact MD, sweeping gas MD, air gap MD, and vacuum membrane distillation (VMD) are used rapidly for various applications (desalination, water-reuse, food, medical, etc.). The resulting driving force of vapor pressure difference produces a flux of water vapor through the membrane, and thus, aqueous brine solutions can be concentrated and crystallized. This process can work on high solute concentration at feed side, at low concentration gradients, moderate temperature, and atmospheric pressure [6].

The benefits of VMD compared to other more popular separation processes are theoretically 100% rejection of ions, colloids, macro molecules, and other nonvolatiles, lower operating pressure than conventional pressure-driven membrane separation processes, lower operating temperature than conventional distillation, and reduced vapor pressure compared to conventional distillation processes. VMD differs from the other membrane technologies in that the driving force for desalination is the difference in vapor pressure of water across the membrane, rather than total pressure.

In VMD, the feed stream contacts directly with the surface of membrane, is maintained at pressure lower than the minimum liquid entry pressure (LEP). LEP is defined as the minimum mass transfer pressure required for an aqueous solution to enter into dry membrane pores, and which should be as high as possible [7]. VMD configuration is shown in Fig. 1. In this configuration, the vapor permeated does not condense in cooling chamber, but is drawn out by vacuum and condenses externally in a condenser. The pressure difference between the two sides of the membrane creates a convective mass flow along the pores that contribute to the total mass transfer for VMD.

In recent research, various theoretical models have been developed for VMD. The main purpose of these models was to predict the values of the permeate flux and its dependence on the membrane module design, membrane parameters, and operating variables [8–26]. A comprehensive review on MD modeling has been reported by Lawson and Lloyd [27]. Many researchers [11,27–32] have used the mathematical models based on gas permeation through a porous membrane comprising Knudsen flow, while others [23,27,33] have employed the model based on the combination of Knudsen–Poiseuille flow to calculate the VMD flux. The various models are compared in Table 1.

The phenomenological models are complicated because of microscopic phenomena occurring in the membrane. The calculation of temperature at membrane surface on feed side (T_{fm}) is difficult to predict by first principle model. The membrane surface temperature on feed side is an important parameter affecting the permeate flux. Several authors have assumed this temperature same as the feed bulk temperature. In this work, computational fluid dynamic (CFD) has been used to compute the feed-side membrane surface temperature. To the best of the knowledge, no work has been reported, which uses CFD in the mathematical modeling to compute the surface temperature. Since the feed flow rate also affects the permeate flux, therefore, this parameter has also been considered in CFD to compute the surface temperature.

The present model considers Knudsen, molecular, and Poiseuille flow transport mechanisms. Most of the authors assumed only Knudsen diffusion or Knudsen–Poiseuille in their model as discussed in Table 1. However, in a paper by Fan and Peng [36], the authors assumed the three mechanisms simultaneously. In their paper, the membrane surface

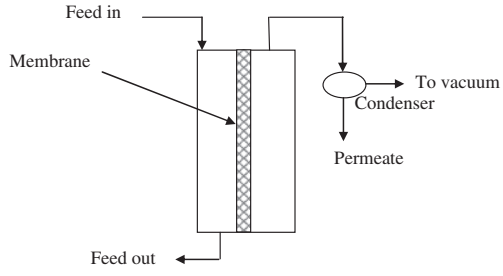

Fig. 1. VMD configuration.

Table 1
Comparison of different models in terms of assumptions and merits/demerits

	Dusty gas model	Knudsen–viscous transition model
Assumptions	Knudsen diffusion was assumed	
	Feed bulk temperature was considered to be the same as feed-side membrane surface temperature	Feed bulk temperature was considered to be the same as feed-side membrane surface temperature
Merits/ demerits	This model gives good fitting at lower feed bulk temperature	
	Poiseuille flow was not considered, hence, the model gives good fit only for Knudsen number greater than one. Permeate flux obtained by this model is less than the experimental since the contribution of Poiseuille flow was neglected in this model	Permeate flux obtained by this model is greater than the experimental
	Effects of feed flow rate and feed salt concentration were not incorporated in the model on permeate flux	Effects of feed flow rate and feed salt concentration were not incorporated in the model on permeate flux
References	[32,34]	[23,27,33,35]

temperature on the feed side was calculated using experimental values of permeate flux, however, in this study, this has been estimated using CFD model in Fluent. Moreover, the feed flow rate also affects the feed-side membrane surface temperature, which in turn influences the permeate flux. Fan and Peng [36] did not estimate the effects of feed flow rate and permeate pressure on permeate flux using mathematical model. However, in this study, these effects have been considered.

The heat loss during the VMD process has been considered as negligible in the models reported by others [23,37]. In this study, the heat loss has also been taken into account. The effects of several operating parameters such as feed flow rate, feed bulk inlet temperature, permeate pressure, salt concentration, and membrane-based parameters such as membrane pore diameter, membrane thickness, and membrane porosity have been studied.

2. Modeling of VMD

The main purpose of this model was to determine the transmembrane flux, its dependency on process-based parameters as well as design variables. In VMD, the process is driven by the temperature difference [38]. The mass transfer in MD consists of two steps: one is across the boundary layer at the feed side; the other is across the membrane.

Assumptions taken in Mathematical Modeling of VMD are as follows:

(a) Vapor permeates through a porous membrane comprising Knudsen diffusion, molecular diffusion, and Poiseuille flow.
(b) The heat loss through membrane is not negligible (effects of conduction and convection in membrane has been considered in present model).
(c) Effect of salt concentration is also included in model equation in terms of activity coefficient using thermodynamic consideration.
(d) Effect of feed flow rate is also incorporated in model by taking into account hydrodynamics as well as heat transfer.
(e) Steady state heat transfer is assumed.

In principle, all the three mechanisms, namely Knudsen diffusion, molecular diffusion, and Poiseuille flow have their influence on mass transfer. The total flux (kmol/m^2 s^{-1}) is given by,

$$N_{A,P-M-K} = N_{A,P} + N_{A,M-K} \quad (1)$$

Mass transfer within membrane pores is regulated by Knudsen diffusion [39] as

$$N_{A,K} = \frac{4}{3} d \frac{\varepsilon}{\tau\delta} \sqrt{\frac{1}{2\pi MRT}} \Delta P \quad (2)$$

The mass flux describing the gas passing through the pores by Poiseuille mechanism [39] is as follows:

$$N_{A,P} = \frac{d^2}{32\eta} \frac{\varepsilon}{\tau\delta} C \Delta P \quad (3)$$

The mass transport of component A due to molecular diffusion is as follows:

$$N_{A,M} = \frac{1}{1 - y_A} \frac{\varepsilon}{\tau \delta RT} D_{AB} \Delta P \quad (4)$$

When $0.01 < K_n$ (Knudsen number) < 1, the corresponding mass transfer coefficient is Knudsen–molecule diffusion transition, in which both the resistance of molecule–pore wall collision and molecule–molecule collision have noticeable influence on mass transfer, but neither of them can predominate exclusively. The total flux is related with $N_{A,M}$ and $N_{A,K}$:

$$1/N_{A,M-K} = (1/N_{A,K}) + (1/N_{A,M}) \quad (5)$$

Combining Eqs. (1)–(5) gives,

$$N_{A,M-K-P} = \frac{\varepsilon}{\tau \delta RT_{fm}} \left\{ \frac{1 - y_A}{D_{AB}} + \frac{3}{4d} \sqrt{\frac{2\pi M}{RT_{fm}}} \right\}^{-1} (P_{fm} - P_{pm}) + \frac{\varepsilon r^2}{\tau \delta} \frac{P_{fm} M}{8 \eta RT_{fm}} (P_{fm} - P_{pm}) \quad (6)$$

The partial pressure of water at the feed-side membrane surface is given by,

$$P_{fm} = (1 - x)\ \gamma\ P^0_{fm} \quad (7)$$

The saturation pressure of water is given by Antoine equation,

$$\ln P^0_{fm} = 23.1964 - \frac{3816.44}{T_{fm} - 46.13} \quad (8)$$

The activity of water in the sodium chloride-water solution is given by Lawson and Lloyd [27]:

$$\gamma = 1 - 0.5x - 10x^2 \quad (9)$$

The heat energy needed for the water to vaporize into the membrane pores is provided by the heat transfer through the boundary layer at the feed side. The heat flux is given by,

$$q_f = h_f (T_f - T_{fm}) \quad (10)$$

Assuming the contribution of both evaporation and conduction, the total heat flux transferred through the membrane is given by,

$$q_m = N\Delta H + h_m (T_{fm} - T_{pm}) \quad (11)$$

The heat flux at the thermal boundary layer at permeate side is given by,

$$q_p = h_p (T_{pm} - T_p) \quad (12)$$

At steady state, these heat fluxes are equal, i.e., $q_f = q_m = q_p$. By solving Eqs. (10)–(12),

$$T_f = \frac{N\Delta H + T_{fm}(h_f + h_m + h_m h_f / h_p) - h_m T_p}{h_f (1 + h_m / h_p)} \quad (13)$$

where T_p can be calculated from Antoine equation corresponding to P_{pm} for water.

The heat transfer coefficient h_p is determined by equating Eqs. (11) and (12) as follows:

$$q_m = q_p = N\Delta H + h_m (T_{fm} - T_{pm}) = h_p (T_{pm} - T_p) \quad (14)$$

From which,

$$h_p = \frac{N\Delta H + h_m (T_{fm} - T_{pm})}{(T_{pm} - T_p)} \quad (15)$$

By estimating the values of T_{fm} and T_{pm} from CFD profile at feed flow rate of 2 lpm, feed bulk temperature of 60°C, and permeate pressure of 5.5 kPa, we get average values of $T_{fm} = 55.36$°C and $T_{pm} = 55.12$°C. Under these conditions, the experimental mass flux is obtained as 26.604 kg/m^2 h. h_m is calculated by the equation $h_m = \frac{(1 - \varepsilon)\lambda_s + \varepsilon \lambda_g}{\delta}$ where λ_s and λ_g are the thermal conductivity of PTFE membrane material and water vapor that fills the pores, respectively. By taking the values of λ_s for PTFE and λ_g as 0.28 and 0.021 W/m °C, respectively [24], we get h_m as 564 W/m^2 °C. T_p is calculated from Antoine equation as 34.8187°C, latent heat of vaporization is 2,358,000 J/kg. The value of h_p is computed to be 865 W/m^2 °C from Eq. (15).

These model equations can be used to predict the mass flux of water vapor through VMD for desalination of water by taking the values of the parameters given in Table 2. For a given membrane characteristics, the performance of VMD can be found by solving the above equations.

2.1. Model for estimation of feed-side membrane temperature

CFD simulation that coupled an established heat and mass transfer model was carried out for the VMD

Table 2
Nominal values of parameters used for desalination of water

Parameter	Value
1-y_A (Mole fraction of air)[a]	1×10^{-5}
M (Molecular weight of water) (kg/kmol)	18
R (Universal gas constant) (J/kmolK)	8,314
λ_{air} (Thermal conductivity of air) (W/m K)	0.021
λ_{PTFE} (Thermal conductivity of PTFE) (W/m K)	0.28
D_{AB} (m^2/s)	2.4×10^{-5}
R (μm)	0.22
Δ (μm)	175
E	0.70
h_m (W/m^2 K)	564

[a]The Henry's constant is 10.1×10^4 atm per mole fraction of air in water at 60°C [40]. Therefore, from the equation $p = Hx$, the solubility of air in water is 1×10^{-5} at atmospheric pressure. It has been assumed that air also gets released while evaporation in the membrane module. Therefore, the mole fraction of air in gaseous mixture is assumed to be 10^{-5}. The same mole fraction of air will reside in pore.

using NaCl solution to predict mass and heat behaviors of the process. The feed-side membrane surface temperature depends on feed bulk temperature, feed flow rate, and permeate pressure. The temperature profile on membrane surface was generated under varied flow rate, feed bulk temperature, and vacuum pressure in Fluent software. The main dimensions of the membrane with test cell module are listed in Table 3.

Fig. 2 schematically shows the geometry of computational domain setup in representing a channel section of the test cell of the membrane module with 200 mm height and diameter of 70 mm. Mesh was generated by the commercial grid-generation tool GAMBIT consisting of 57,871 nodes, and the structured quadrilateral grid was used. A non-uniform mesh was adopted with the mesh density being higher near to the membrane surface. In all cases, the mesh independence of the solution was checked and made sure that there were sufficient cells in the temperature boundary layer. The automatic mesh partition of membrane silk was body fitted anisotropic mesh: The distance from the first mesh point to the boundary was 0.05, called first row; the growth factor was 1.01; and the creating form was 1:1. The more detailed meshes were generated for the import and export of the membrane and the membrane silk vacuum ports. Fluent was used as CFD simulation in this work to evaluate the flow conditions in this membrane module test cell. Fig. 3 shows the flow chart of solution step to calculate the feed-side membrane surface temperature (T_{fm}).

Table 3
Test cell module dimensions

Parameter	Dimension (mm)
Effective membrane diameter	52
Feed section diameter	70
Feed section length	123
Permeate section length	73

In CFD simulation, for instance, the liquid feed was assumed to be aqueous solution of NaCl with concentration of 0.5 mol/l. The feed bulk inlet temperature of 60°C was entered in the software. The inner section was defined as wall except the entry of the membrane silk, so that NaCl aqueous solution can only flow up to the silk where the water molecules of NaCl aqueous solution evaporated, permeating through the membrane pores into the permeate section.

2.2. Boundary and initial conditions

2.2.1. Feed inlet

The inlet region of membrane model was simplified into a rectangular region, which was set to velocity inlet. The inlet pressure was 1 atmospheric pressure, the feed flow rate varied from 0.5 to 2 lpm, and the gravitational acceleration was 9.81 m/s^2.

2.2.2. Pressure outlet

The outlet was set to pressure outlet. For outflow boundary condition, the velocity gradient of fluid was assumed to be zero, and the outlet temperature was 5°C lower than the inlet temperature.

2.2.3. Vacuum exports

Vacuum export was set to pressure outlet, the pressure was in the range of 7–1 kPa, and the backflow of vapor was zero.

2.2.4. Porosity of the membrane silk

The flow through the porous field was calculated using the superficial velocity under the assumptions that membrane silk surface was considered as a wall (ignore the membrane flexibility), and the membrane surface was set to porous jump. Because of membrane thickness much smaller as compared to membrane characteristic size, the membrane was treated as porous jump instead of grid mesh [41]. The parameters of

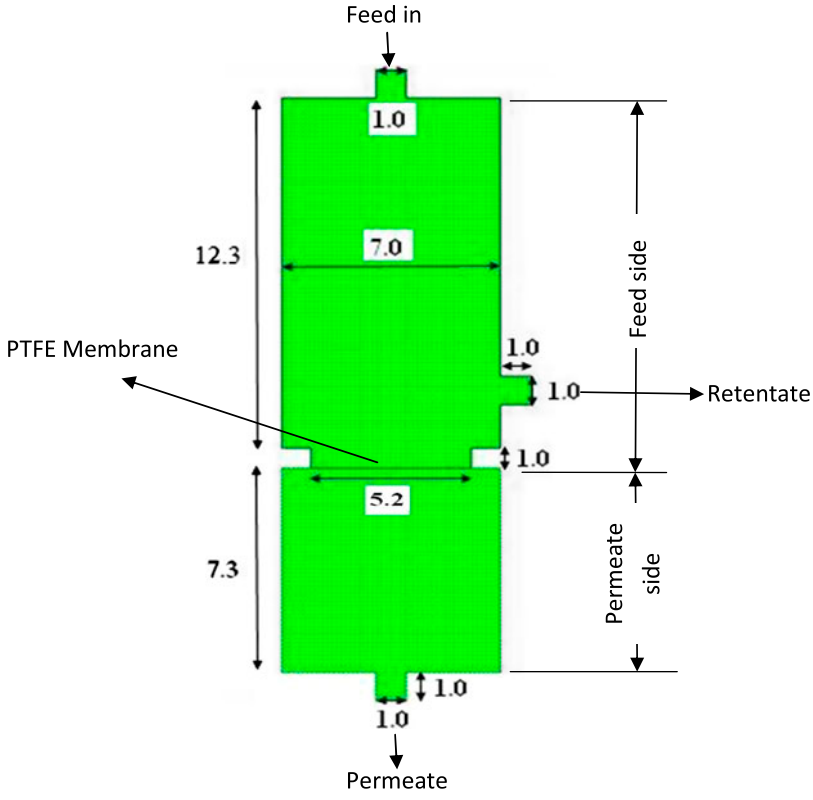

Fig. 2. Membrane module test cell (all dimensions are in cm).

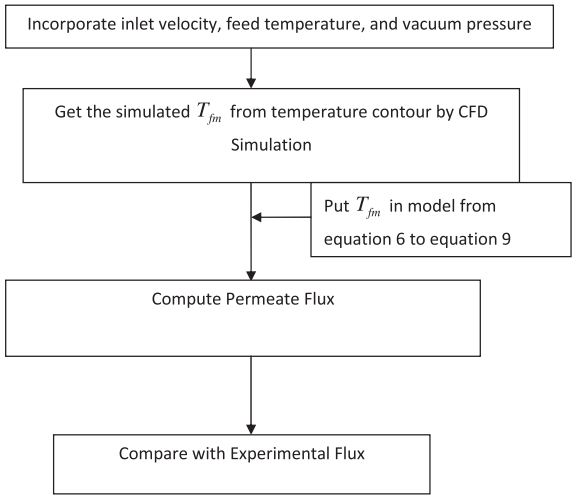

Fig. 3. Flow chart of solution step to calculate the T_{fm}.

porous jump, viz face permeability (α), porous medium thickness (δ), and pressure jump coefficient (c) were determined as follows:

$$\alpha = \frac{\varepsilon^2}{a\tau s^2} = 1.5 \times 10^{-16}\ \mathrm{m}^2$$

$$\delta = 175 \text{ microns}$$

$$c = \frac{2b\tau}{\varepsilon^2 d} = 1.54 \times 10^7\ \mathrm{m}^{-1}$$

where ε, τ, s, and d are porosity, tortuosity, surface per unit volume of membrane, and pore diameter, respectively. The value of a and b are 8.61 and 0.52, respectively [41].

3. Experimental

A laboratory scale VMD setup was used in the study. The schematic diagram of the experimental setup is shown in Fig. 4. A flat sheet hydrophobic microporous PTFE membrane with an effective area of 0.00212 m^2 was used for the experiments. The feed water was heated to the required temperature 40–70°C using a heating apparatus (heater) at base of the feed tank. The feed solution was then pumped from the feed tank by a feed pump (0.37/0.50 HP of Crompton make) to the membrane unit. The feed was circulated through the membrane module. The feed flow rate was maintained using rotameter installed before the

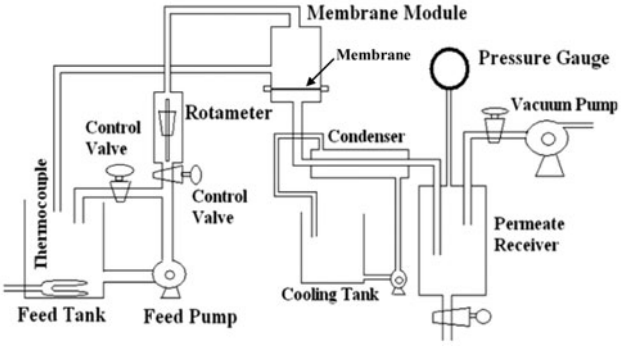

Fig. 4. Schematic diagram of VMD setup.

membrane unit. The temperature of both fluids of inlet and outlet was monitored using digital thermometers. A vacuum pump (FRACOVAC make) was installed at base to create the required vacuum at permeate side by which the partial pressure difference across the membrane was maintained. A distillation unit was used at permeate side to condense the vapor coming from the membrane unit. A cold water reservoir was housed in the setup to supply cold water to the VMD unit. A permeate receiver was used to collect the condensed water. A pressure gauge was used to measure the vacuum created.

3.1. Experimental procedure

PTFE membrane was purchased from Millipore, the characteristics of which are given in Table 4. The experiments of VMD were carried out using a hydrophobic PTFE microporous flat sheet membrane. The aqueous feed solution of salt was prepared and continuously fed through a feed tank to the membrane module by feed pump. On the permeate side of the membrane module, the vacuum pump was connected. The permeate water vapor was condensed continuously in a condenser. The membrane flux was measured by collecting permeate in a graduated receiver. The temperature controller equipped with heater was connected to maintain the temperature of the feed solution in the feed tank. Electrical conductivity of the distillate permeate was measured using a conductivity meter.

Table 4
Membrane characteristics

Properties	Specifications
Membrane material	PTFE
Surface property	Hydrophobic
Diameter (mm)	90
Effective membrane diameter (mm)	52
Pore size (μm)	0.22
Thickness (μm)	175
Porosity (%)	70
Effective membrane area (m^2)	0.00212
Maximum operating temperature (°C)	130
Supplier	Millipore

4. Results and discussion

To study the effect of various parameters, experiments were carried out at different flow rates in the range of 0.5–2.0 lpm and the feed bulk temperature range of 40–60°C, feed salt concentration of 20,000 ppm at varied permeate pressure.

4.1. Effect of feed flow rate on permeate flux

The trend of variation in permeate flux with variation in feed flow rate at different feed bulk temperature is shown in Fig. 5. It can be observed that the permeate flux increases on increasing feed flow rate. The possible reason for increase in permeate flux with increase in feed flow rate at constant feed inlet temperature might be decrease in temperature and concentration boundary layer due to increase in N_{Re}. It can also be seen that the flux increases linearly at low temperature with increase in feed flow rate but it increases as S-shaped profile at higher temperatures 55 and 60°C. The probable reason for S-shaped profile is that T_{fm} is closer to T_f at high flow rates causing flux less sensitive to changes in flow rate. However, at lower feed bulk temperature, the difference between T_{fm} and T_f is smaller; therefore, permeate flux does

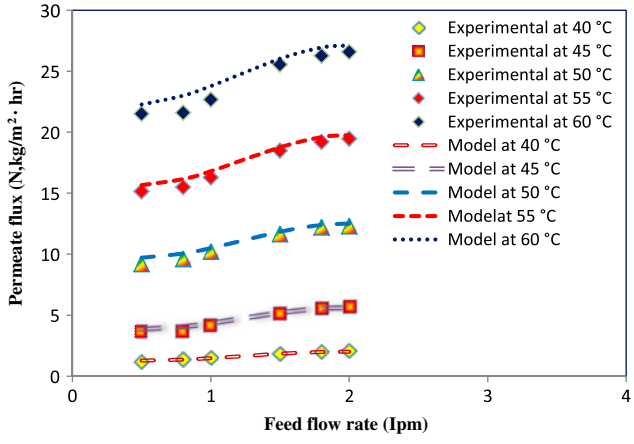

Fig. 5. Effect of feed flow rate on permeate flux (5.5 kPa of permeate pressure and feed salt concentration of 20,000 ppm).

Table 5
Effect of feed flow rate on permeate flux (at 20,000 ppm NaCl salt concentration and 5.5 kPa of permeate pressure)

Feed flow rate (lpm)	Feed bulk temperature (°C)	R^2	MAPE (%)
0.5–2	40	0.991	3.24
0.5–2	45	0.992	3.76
0.5–2	50	0.998	2.92
0.5–2	55	0.998	2.54
0.5–2	60	0.987	3.49

not change much on increasing the feed flow rate. Beyond 2 lpm, no significant effect was observed on flux. The linear increment in permeate flux was also reported by others [10,11,23,24,42] at low feed temperature, whereas Xu et al. [33] have reported the linear increment at lower temperature and cubic (S-shaped) increment in permeate flux with increasing feed flow rate at higher feed inlet temperature. The flux data at different feed flow rate and temperature were also determined using the mathematical model developed in this study and presented by continuous line in Fig. 5.

The closeness of predicted and experimental data has been calculated by estimation of two statistical parameters R^2 and mean absolute percentage error (MAPE). As shown in Table 5, R^2 found in the range of 0.981 to 0.998 and MAPE was found in the range of 2.54 to 3.76. It shows a good match between the predicted and experimental data of flux.

4.2. Effect of feed bulk inlet temperature on permeate flux

Fig. 6 illustrates the performance of VMD at different feed temperature (45, 50, 55, and 60°C) under different conditions of feed flow rate (0.5,1, and 2 lpm) at constant pressure of 7 kPa and 20,000 ppm of feed salt (NaCl) concentration. It was observed that the experimental permeate flux increases gradually with increasing feed bulk inlet temperature under different varied feed flow rate. This is attributable to the fact that the feed-side vapor pressure increases on increasing feed temperature.

It was also found that the VMD transmembrane permeate flux was 25.6, 22.4, and 20.1 kg/m^2 h at 2,1, and 0.5 lpm, respectively, at 60°C of feed bulk inlet temperature. Moreover, it is also easy to visualize that the increment in transmembrane flux is more rapid on increasing the feed bulk temperature as compared to feed flow rate. As shown in Table 6, the value of R^2 (0.999) and MAPE (0.59–2.2%) indicates a very good match between predicted and experimental flux data with variation in feed inlet temperature.

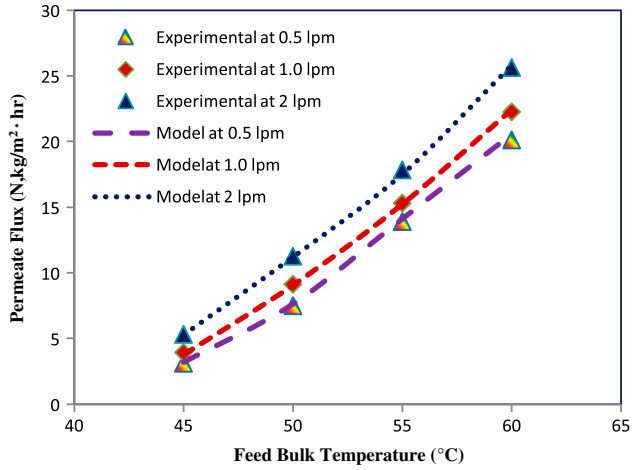

Fig. 6. Effect of feed bulk temperature on permeate flux (permeate pressure of 7 kPa and feed salt concentration of 20,000 ppm).

Table 6
Effect of feed bulk inlet temperature on permeate flux (at 20,000 ppm of NaCl salt concentration and 7 kPa of permeate pressure)

Feed inlet temperature (°C)	Feed flow rate (lpm)	R^2	MAPE (%)
45–60	0.5	0.999	2.2
45–60	1	0.999	1.1
45–60	2	0.999	0.59

The present model has been compared with the model of Mericq et al. [34] as shown in Table 7. Mericq et al. [34] assumed dusty gas model comprising Knudsen diffusion in which the feed bulk temperature was assumed same as feed-side membrane temperature. The permeate flux obtained by present model showed higher value than that reported by Mericq et al. [34]. This is because Mericq et al. [34] ignored Poiseuille contribution in their model; however, the current model takes into consideration of Knudsen, molecular, and Poiseuille flow. Although, R^2 value for both the models is same, the MAPE value obtained by present model is 1.9% which is far less than the value of MAPE (9.2%) obtained by Mericq et al. [34] model. This clearly indicates that the present model has provided a better fitting between the predicted and experimental data of flux.

The fractional contribution of Poiseuille flow has also been calculated as shown in Fig. 7. As the feed bulk temperature increases, Poiseuille contribution increases due to higher rate of vaporization. The Poiseuille contribution increases from 7.2 to 14.2% on

Table 7
Comparative study of effect of feed bulk temperature (permeate pressure of 5 kPa and feed flow rate of 5 lpm)

Feed bulk temperature (°C)	Experimental flux (kg/m^2 h)	Predicted flux (kg/m^2 h)		R^2 (1)	R^2 (2)	MAPE (1)	MAPE (2)
		(1)	(2)				
40	2.1	2.4	2.59	0.999	0.999	9.2	1.9
45	5.5	4.4	4.80				
50	13.1	11.2	12.40				
55	23.4	20.8	23.43				
60	32.1	29.4	33.48				
65	45.6	39.73	45.91				
70	60	53.11	61.90				

Notes: (1)—obtained using dusty gas model [34].
(2)—obtained using present model.

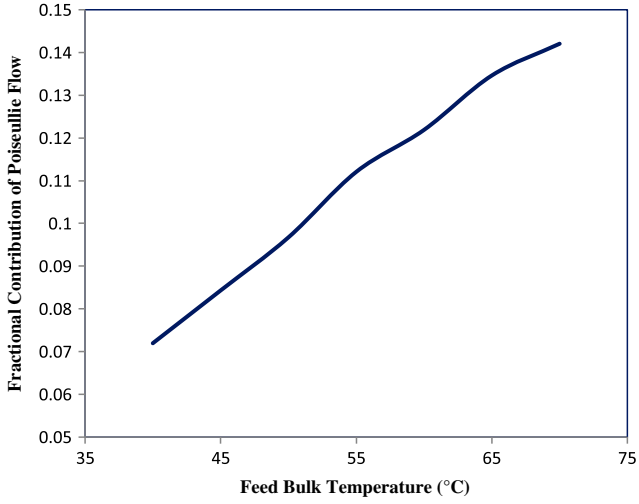

Fig. 7. Effect of feed temperature on fractional contribution of Poiseuille flow.

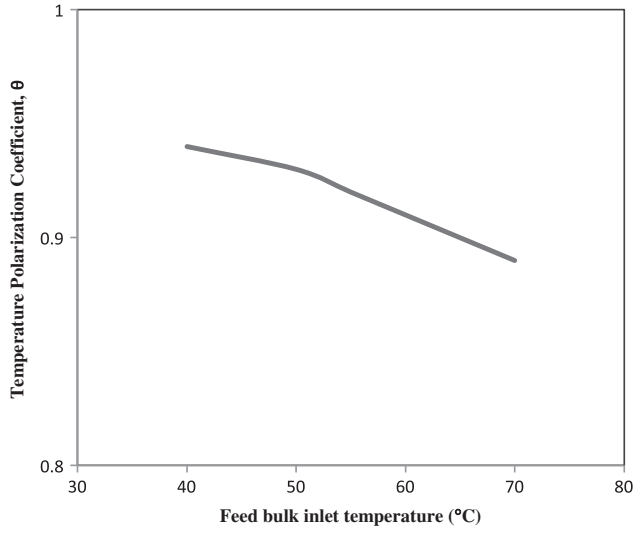

Fig. 8. Effect of feed bulk inlet temperature on TPC.

increasing feed bulk temperature from 40 to 70°C, i.e., approximately 0.23% rise per °C.

The temperature polarization coefficient (TPC) is defined as the ratio of feed-side membrane surface temperature (feed–membrane interface) to the feed bulk inlet temperature for nonvolatile solute component present in aqueous solution. It is calculated as follows:

$$\theta = \frac{T_{\mathrm{fm}}}{T_{\mathrm{f}}} \tag{16}$$

It is found from Fig. 8 that TPC decreases with increasing feed bulk inlet temperature at permeate pressure of 5.5 kPa and feed inlet flow rate of 2 lpm, which causes decrease in thermal boundary layer at high feed bulk inlet temperature and subsequent increase in permeate flux.

4.3. Effect of permeate pressure on flux

The basic driving force for VMD is the vapor pressure difference across the membrane and can be maintained either by creating a temperature difference or by applying vacuum on the permeate or downstream side of the membrane. To study the effect of permeate side operating pressure as vacuum, experiments have been carried out at feed flow rate of 2 lpm, feed bulk temperature of 55 and 60°C, and feed salt (NaCl) concentration of 20,000 ppm. The results are presented in

Fig. 9. From the figure, it can be seen that the experimental permeate flux decreases with respect to increase in permeate pressure or in other words, the flux has shown increasing trend with increase in vacuum pressure. The permeate flux varied from 26.6 to 25.6 kg/m^2 h with variation in permeate pressure from 5.5 to 7 kPa, (i.e., vacuum of 94.5–93 kPa) at feed flow rate of 2 lpm, and feed bulk inlet temperature of 60˚C.

This increase of permeate flux was due to increase of the vapor pressure difference by increasing the degree of vacuum at constant feed bulk temperature as a result it increases the vapor pressure of water which directly increased the driving force for mass transfer. Also, the mass transfer resistance gets reduced by decreasing the permeate pressure on the downstream side since the vacuum increases the driving force for Knudsen–molecule transition and Poiseuille flow.

The trend of variation of VMD flux with variation in permeate pressure is S-shaped or sometimes inverted S-shaped. In this figure, the behavior is inverted S-shaped. This behavior is due to the corresponding increase in vapor pressure of water as exponential dependence of water vapor pressure on feed bulk inlet temperature by Antoine equation, and it may be attributed to additional convective flow (Poiseuille) caused by the total pressure difference. This non-linear relationship may be due to the implicit relation between the permeate flux and vapor pressure difference. This type of trend as well as positive increment in permeate flux with increase in vacuum pressure was also reported by others [11,28,29,34,43].

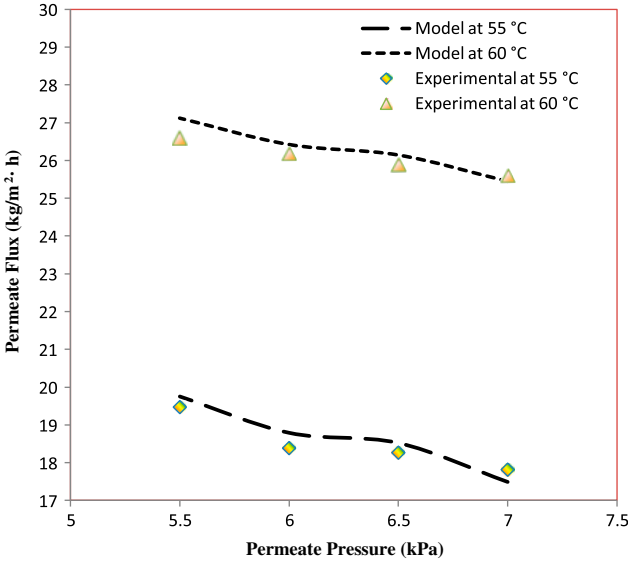

Fig. 9. Effect of permeate pressure on permeate flux at feed flow rate of 2 lpm.

The mathematical model developed in this work was also found in reasonable agreement with experimental data as shown in Fig. 9. R^2 value ranged from 0.97 to 1 and MAPE ranged from 0.9 to 1.7%, as shown in Table 8, further confirms the goodness of fitting of mathematical model with experimental data.

At different permeate pressures, flux has been calculated using the present model and also by Zhongwei et al. [35] and the comparison of flux data with experimental data are compared in Table 9. Flux calculated by the present model shows lower value as compared to that reported by Zhongwei et al. [35] as the feed-side membrane surface temperature in the current model has been calculated lower than feed bulk temperature whereas Zhongwei et al. [35] assumed this temperature same as feed bulk temperature. Moreover, the molecular diffusion may have also contributed slightly higher permeate flux. Although R^2 values are almost the same for both the models, but the MAPE value of the present model is far less (3.6) compare to Zhongwei model (12.7). It clearly shows that the current model has shown much better fitting of predicted data with experimental data. The trend of variation in predicted data and experimental data is shown in Fig. 10.

4.4. Effect of feed concentration on permeate flux

The experiments were conducted for various NaCl salt concentrations at feed flow rate of 2 lpm, and permeate pressure of 6 kPa, at different feed bulk temperature of 55 and 60˚C as shown in Fig. 11.

It is found from Fig. 11 that the experimental permeate flux slightly decreases with increasing feed inlet concentration from 5 to 20 g/l. This decrement was less than 1 and 2% for 55 and 60˚C feed bulk inlet temperature, respectively. This shows that there is negligible effect of increasing salt concentration on permeate flux. However, this effect was not negligible when the feed concentration was raised to sea water, i.e., 30–40 g/l. It was observed that the declination of permeate flux was nearly 15 and 10% at 55 and 60˚C

Table 8
Effect of permeate pressure on permeate flux (at 20,000 ppm NaCl salt concentration, 2 lpm feed flow rate)

Permeate pressure (kPa)	Feed bulk temperature (˚C)	R^2	MAPE
5.5–7	55	0.92	1.7
5.5–7	60	0.96	0.9

Table 9
Comparative study of effect of permeate pressure (feed bulk temperature of 60°C, and feed velocity of 0.290 m/s)

Permeate pressure (kPa)	Experimental flux of Zhongwei ding et al. [35] (kg/m^2 h)	Predicted flux (kg/m^2 h)		R^2 (1)	R^2 (2)	MAPE (1)	MAPE (2)
		(1)	(2)				
Assumption: Knudsen–viscous transition							
14	20.98	26.47	22.28	0.998	0.999	12.7	3.6
12	34	37.93	34.78				
10	46.8	51.37	48.32				
8	57.2	62.83	58.71				
6	69	75.78	70.95				
4	78.8	88.23	81.98				
2	92.7	101.68	96.32				

Notes: (1)—obtained using Knudsen–viscous transition [35].
(2)—obtained using present model.

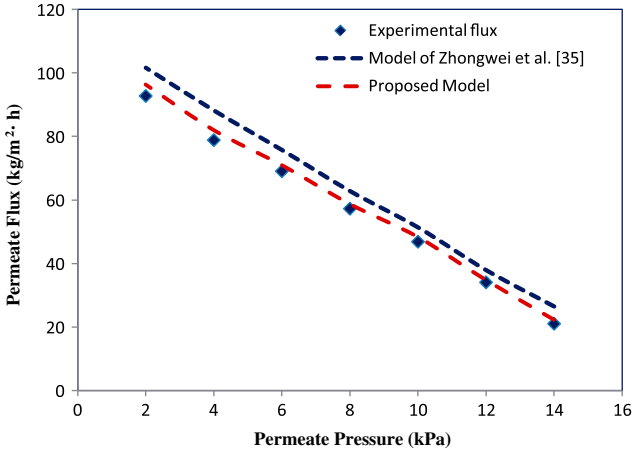

Fig. 10. Effect of permeate pressure on permeate flux.

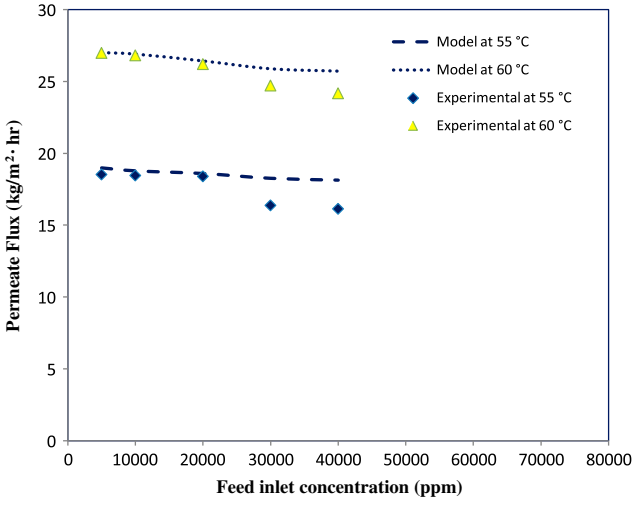

Fig. 11. Effect of feed salt concentration on permeate flux.

feed bulk inlet temperature respectively. The reduction in permeate flux on increasing salt concentration has also been reported by [44]. Increasing the concentration of nonvolatile solutes in the form of salt in the feed solution results in the declination of permeate flux due to the decrease of water vapor pressure with the salt addition which may affect the driving force for mass transfer. Moreover, at higher salt concentration, the extra boundary layer is created on the surface of membrane–feed interface. This problem can be minimized by creating the turbulence or increasing the feed flow rate for enhancing the VMD performance. Hence, the performance of VMD was different for low salt concentration and high salt concentration. However, due to low salt concentration in ground water, the permeate flux will not change significantly. Sometimes this reduction of permeate flux at high salt concentration leads to the crystallization and scaling on membrane surface. But, it was observed that effect of scaling in water desalination through VMD was not very strong. This outcome was also supported by Mohammadi and Safavi [45]. Due to this reason, VMD can be used for desalination of higher salt concentration as compared to other membrane process like reverse osmosis (RO) without altering a huge drop in production. Since concentration polarization is very

Table 10
Effect of feed inlet concentration on permeate flux (at permeate pressure of 6 kPa, 2lpm feed flow rate)

Feed inlet concentration (ppm)	Feed bulk temperature (°C)	R^2	MAPE
5,000–40,000	55	0.91	5.84
5,000–40,000	60	0.97	2.47

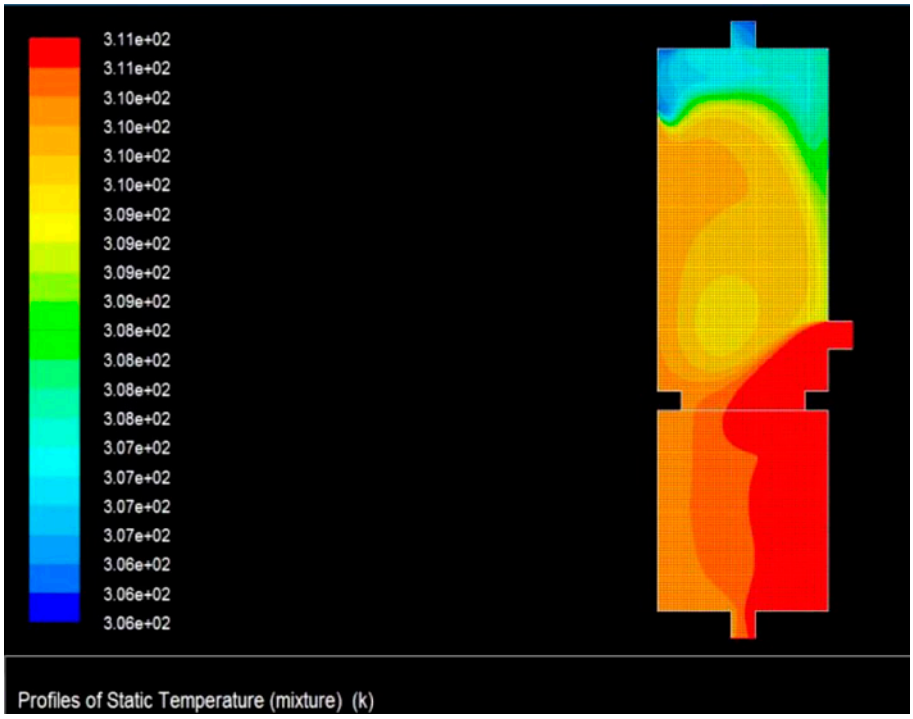

Fig. 12. Temperature profile of membrane module at 40℃ of feed bulk temperature.

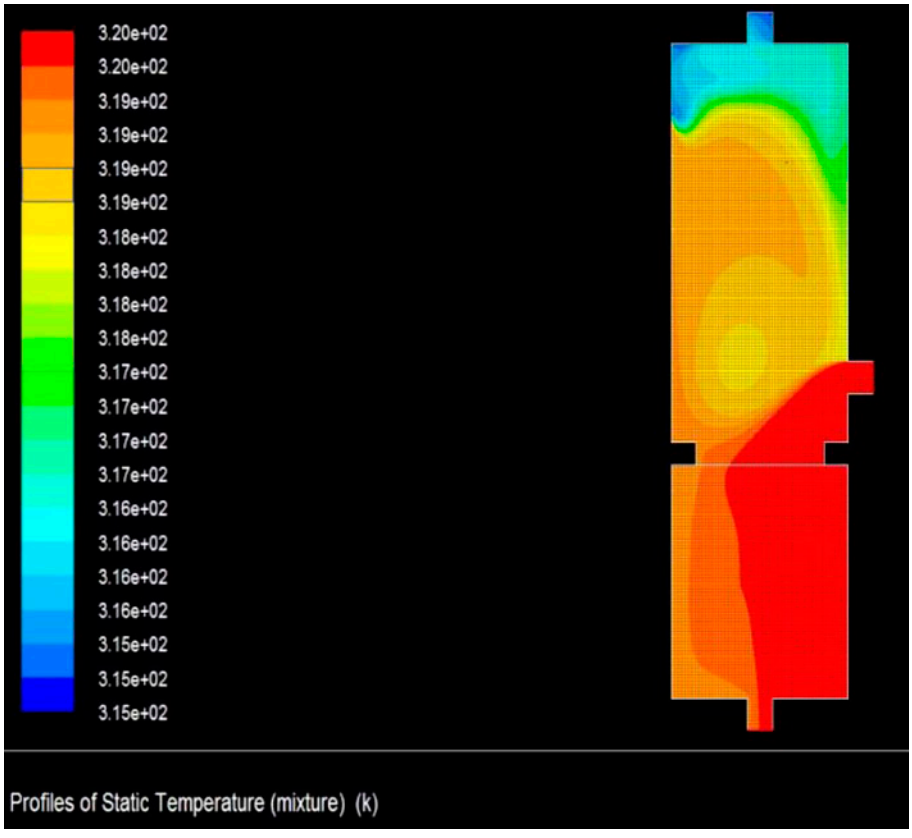

Fig. 13. Temperature profile of membrane module at 50℃ of feed bulk temperature.

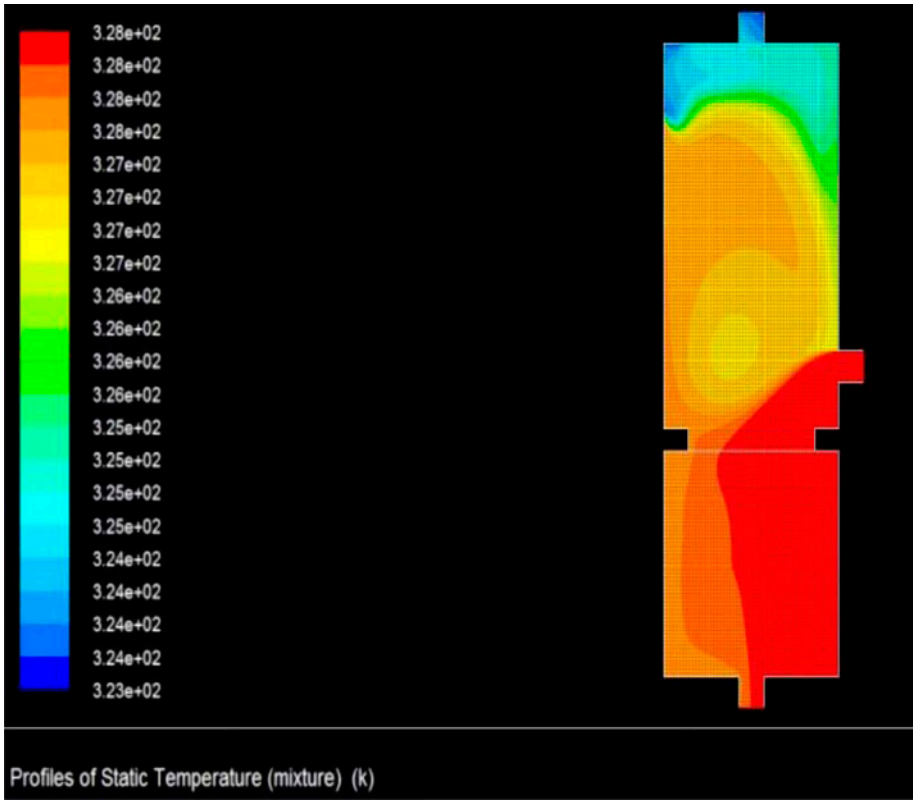

Fig. 14. Temperature profile of membrane module at 60˚C of feed bulk temperature.

large in RO, which ultimately creates reduction in permeate flux to a large extent in RO as compared to the VMD.

The mathematical model values were compared with experimental result, which are found in well agreement. The R^2 and MAPE values are shown in Table 10.

Based on the above discussion of the effects of various parameters, the optimum values at which the permeate flux is found to be maximum are permeate pressure of 5.5 kPa, feed temperature of 60˚C, and feed flow rate of 2 lpm.

4.5. CFD results

In this work, CFD has been applied to estimate the temperature at the feed-side membrane surface as it is difficult to install a temperature sensor at the membrane. The detailed description of this method has already been described in Sections 2.1 and 2.2. The grid was generated in GAMBIT consisting of 57,871 nodes and the quadrilateral structure. A non-uniform mesh with finer grid at the membrane surface was used. A multiphase mixture model was assumed with three phases consisting of water, vapor, and air. In the solver, the options considered are as follows: pressure-based solver, 2-D, absolute velocity formulation, Green-Gauss cell based gradient option, implicit formulation, steady state model, and superficial velocity porous formulation. Energy equations were also considered in the calculation. In the viscous model, k-epsilon (two equations) with realizable conditions was adopted. Operating pressure of 101,325 Pa and gravity effect was considered in the operating conditions.

The equations such as continuity equation, x-velocity, y-velocity, energy, k, and epsilon were solved in Fluent. The temperature profiles in the membrane module were generated at varied permeate pressure in the range of 5.5–7.0 kPa, feed bulk temperature in the range of 40–60˚C, and feed flow rate of 0.5–2 lpm. Figs. 12–14 represent the temperature profiles at 40, 50, and 60˚C, respectively, at feed flow rate of 2 lpm and 5.5 kPa of permeate pressure. The estimated temperature by the Fluent at the feed-side membrane surface (T_{fm}) was used for further calculation in this work.

Table 11
Separation (% rejection) of different ions by VMD for simulated ground water sample

Parameters	Concentration in feed (ppm)	Concentration in permeate (ppm)	Percentage rejection
Ca^{++}	327	2.61	99.2
Mg^{++}	126.3	0.63	99.5
Na^{+}	431.2	0.43	99.9
K^{+}	193	0.96	99.5
Cl^{-}	1,147.5	1.14	99.9
SO_4^{--}	668.6	2.67	99.6
Fe^{++}	18.4	0.16	99.1
NO_3^{-}	306.9	2.45	99.2
F^{-}	113	0.67	99.4

4.6. Study on rejection of multi-ions in the feed (simulated equivalent to ground water)

Besides aqueous solution of NaCl, ground water having multi-ions was also studies for ions rejection in VMD since ground water is essential and vital component of our life support system. Fluoride, iron, nitrates, phosphates, and heavy metals are the commonly observed contaminants in ground water. The average range of toxic contaminants in ground water of Indian states has been reported by Pangarkar et al. [32]. The permissible limits are given in the report of ministry of water resource, Government of India (http://wrmin.nic.in/writereaddata/linkimages/wq11955194163.pdf). Multi-ions feed water sample was prepared by adding $CaCl_2$, $MgCl_2$, NaCl, NaF, $FeSO_4$, and $NaNO_3$. The ions concentration is given in Table 11. The experimental work for removal of different ions (Ca^{++}, Mg^{++}, Na^{+}, K^{+}, Cl^{-}, SO_4^{--}, Fe^{++}, NO_3^{-}, F^{-}) through VMD was carried out, and the experimental results are shown in Table 11. The concentration of different ions in permeate was found within permissible limits as per World Health Organization standards [46] and Indian Standard guidelines. The percentage rejection was found to be more than 99% in all cases.

This constant value of percentage rejection was due to the negligible fouling phenomena. It clearly indicates strong possibility of using VMD for removal of various ions from the water.

5. Conclusions

A mathematical model was developed based on molecular–Knudsen diffusion and Poiseuille flow. CFD simulation was carried out for determination of feed-side membrane temperature. The permeate flux was computed by this model by varying the operating parameters such as feed flow rate, feed bulk temperature, permeate pressure, and feed salt concentration. The computed and experimental results were fitted well with R^2 and MAPE values in the range of 0.991–0.999 and 0.59–3.76, respectively. The model developed in this study has also been compared with dusty gas model results.

It was observed that the permeate flux increased from 21.52 to 26.6 kg/m^2 h on increasing the feed flow rate from 0.5 to 2 lpm at 5.5 kPa of vacuum pressure, 60°C of feed bulk temperature and 20 g/l NaCl salt concentration. The gradual increment was observed in the experimental permeate flux from 5.3 to 25.61 kg/m^2 h with increasing feed bulk inlet temperature from 45 to 60°C at feed flow rate of 2 lpm. The contribution of Poiseuille flow for the permeate flux was found to be increased from 7 to 14% with increase in feed bulk temperature from 40 to 70°C but it does not dominate over Knudsen diffusion. The permeate flux showed the variation from 17.8 to 19.5 kg/m^2 h on decreasing permeate pressure from 7 to 5.5 kPa. Only 2% of decrement in flux was observed with increase in salt concentration from 5 to 20 g/l at 60°C of feed bulk temperature. And this declination of permeate flux reached to 15%, when the feed concentration was raised equivalent to sea water, i.e., 30–40 g/l of NaCl at 60°C. Rejection for NaCl at different concentrations was observed to be more than 99%. Rejection for multi-ion feed water equivalent to ground water was also found to be more than 99%.

List of Symbols

C — total concentration of the gas
D — membrane pore diameter (m)
D_{AB} — diffusivity of A in B (m^2/s), where A is water vapor, and B is air
ΔH — latent heat of vaporization of water (J/kmol)
h_m — membrane heat transfer coefficient (W/m^2 K)
h_p — permeate-side heat transfer coefficient (W/m^2 K)

h_f	—	feed-side heat transfer coefficient (W/m^2 K)
M	—	molecular weight of water (kg/kmol)
N or $N_{A,P\text{-}M\text{-}K}$	—	total transmembrane flux (kmol/m^2 s)
$N_{A,P}$	—	flux due to Poiseuille flow (kmol/m^2s)
$N_{A,K}$	—	Knudsen diffusion (kmol/m^2 s)
$N_{A,M}$	—	molecular diffusion (kmol/m^2 s)
ΔP	—	pressure difference across the membrane
P_{pm}	—	permeate-side membrane pressure (kPa)
P_{fm}	—	feed-side membrane pressure (kPa)
P^0_{fm}	—	feed-side membrane pressure (kPa)
q_f	—	heat flux at feed side (J/m^2•s)
q_m	—	heat flux through membrane (J/m^2 s)
q_p	—	heat flux at permeate side (J/m^2 s)
R	—	universal gas constant (J/kmol K)
r	—	membrane pore radius (m)
T_f	—	feed bulk temperature (K)
T_{fm}	—	feed-side membrane surface temperature (K)
T_p	—	temperature corresponding to permeate pressure (K)
T_{pm}	—	permeate-side membrane surface temperature (K)
x	—	mole fraction of salt NaCl
y_A	—	mole fraction of water vapor

Greek letters

γ	—	activity coefficient of water in sodium chloride solution
δ	—	membrane thickness (m)
ε	—	membrane porosity
η	—	viscosity of water vapor (kg/m s)
θ	—	temperature polarization coefficient
τ	—	membrane tortuosity

References

[1] J. Kurbiel, W. Balcerzak, S.M. Rybicki, K. Świst, Selection of the best desalination technology for highly saline drainage water from coal mines in southern Poland, Desalination 106 (1996) 415–418.

[2] L. Mariah, C.A. Buckley, C.J. Brouckaert, D. Jaganyi, E. Curcio, E. Drioli, Membrane distillation for the recovery of crystalline products from concentrated brines, in: WISA Biennial Conference, Durban, South Africa, May 21–25, 2006.

[3] M.S. Khayet, T. Matsuura, Membrane Distillation: Principles and Applications, Elsevier, Amsterdam, 2011.

[4] M. Mulder, Basic Principles of Membrane Technology, Springer, Dordrecht, 1996.

[5] R. Baker, Membrane Technology and Applications, second ed., John-Wiley & Sons Ltd., Chichester, 2004.

[6] L. Mariah, Membrane distillation of concentrated brines, Ph.D., Dissertation, University of KwaZulu-Natal, Durban, School of Chemical Engineering, 2006.

[7] M.A.E.-R. Abu-Zeid, Y. Zhang, H. Dong, L. Zhang, H.-L. Chen, L. Hou, A comprehensive review of vacuum membrane distillation technique, Desalination 356 (2015) 1–14.

[8] A.M. Alklaibi, N. Lior, Membrane-distillation desalination: Status and potential, Desalination 171 (2005) 111–131.

[9] F.A. Banat, J. Simandl, Theoretical and experimental study in membrane distillation, Desalination 95 (1994) 39–52.

[10] S. Bandini, C. Gostoli, G.C. Sarti, Separation efficiency in vacuum membrane distillation, J. Membr. Sci. 73 (1992) 217–229.

[11] S. Bandini, G.C. Sarti, Heat and mass transport resistances in vacuum membrane distillation per drop, AIChE J. 45 (1999) 1422–1433.

[12] M.N. Chernyshov, G.W. Meindersma, A.B. de Haan, Modelling temperature and salt concentration distribution in membrane distillation feed channel, Desalination 157 (2003) 315–324.

[13] Z. Ding, R. Ma, A.G. Fane, A new model for mass transfer in direct contact membrane distillation, Desalination 151 (2003) 217–227.

[14] F.A. Banat, J. Simandl, Desalination by membrane distillation: A parametric study, Sep. Sci. Technol. 33 (1998) 201–226.

[15] P.J. Foster, A. Burgoyne, M.M. Vahdati, Improved process topology for membrane distillation, Sep. Purif. Technol. 21 (2001) 205–217.

[16] M. Gryta, M. Tomaszewska, Heat transport in the membrane distillation process, J. Membr. Sci. 144 (1998) 211–222.

[17] M. Gryta, M. Tomaszewska, A.W. Morawski, Membrane distillation with laminar flow, Sep. Purif. Technol. 11 (1997) 93–101.

[18] M. Khayet, P. Godino, J.I. Mengual, Theory and experiments on sweeping gas membrane distillation, J. Membr. Sci. 165 (2000) 261–272.

[19] M. Khayet, T. Matsuura, Pervaporation and vacuum membrane distillation processes: Modeling and experiments, AIChE J. 50 (2004) 1697–1712.

[20] K.W. Lawson, D.R. Lloyd, Membrane distillation. II. Direct contact MD., J. Membr. Sci. 120 (1996) 123–133.

[21] L. Martínez, F.J. Florido-Diaz, A. Hernandez, P. Pradanos, Characterisation of three hydrophobic porous membranes used in membrane distillation: Modelling and evaluation of their water vapour permeabilities, J. Membr. Sci. 203 (2002) 15–27.

[22] L. Martínez-Díez, M.I. Vázquez-González, Temperature and concentration polarization in membrane distillation of aqueous salt solutions, J. Membr. Sci. 156 (1999) 265–273.

[23] J.I. Mengual, M. Khayet, M.P. Godino, Heat and mass transfer in vacuum membrane distillation, Int. J. Heat Mass Transfer 47 (2004) 865–875.

[24] J. Phattaranawik, R. Jiraratananon, A.G. Fane, Heat transport and membrane distillation coefficients in direct contact membrane distillation, J. Membr. Sci. 212 (2003) 177–193.

[25] Z. Xiuli, Z. Weidong, H.A.O. Xinmin, Z. Huifeng, Z. Zeting, Z. Jianchun, Mathematical model of gas permeation through PTFE porous membrane and the effect of membrane pore structure, Chinese J. Chem. Eng. 11 (2003) 383–387.

[26] C.K. Chiam, R. Sarbatly, Vacuum membrane distillation processes for aqueous solution treatment—A review, Chem. Eng. Process. 74 (2013) 27–54.
[27] K.W. Lawson, D.R. Lloyd, Membrane distillation, J. Membr. Sci. 124 (1997) 1–25.
[28] F. Banat, F.A. Al-Rub, K. Bani-Melhem, Desalination by vacuum membrane distillation: Sensitivity analysis, Sep. Purif. Technol. 33 (2003) 75–87.
[29] S. Bandini, A. Saavedra, G.C. Sarti, Vacuum membrane distillation: Experiments and modeling, AIChE J. 43 (1997) 398–408.
[30] S. Bouguecha, R. Chouikh, M. Dhahbi, Numerical study of the coupled heat and mass transfer in membrane distillation, Desalination 152 (2003) 245–252.
[31] M.A. Izquierdo-Gil, G. Jonsson, Factors affecting flux and ethanol separation performance in vacuum membrane distillation (VMD), J. Membr. Sci. 214 (2003) 113–130.
[32] B.L. Pangarkar, S.B. Parjane, R.M. Abhang, M. Guddad, The heat and mass transfer phenomena in vacuum membrane distillation for desalination, Int. J. Chem. Biomol. Eng. 3 (2010) 33–38.
[33] Z. Xu, Y. Pan, Y. Yu, CFD simulation on membrane distillation of NaCl solution, Front. Chem. Eng. Chin. 3 (2009) 293–297.
[34] J.P. Mericq, S. Laborie, C. Cabassud, Vacuum membrane distillation for an integrated seawater desalination process, Desalin. Water Treat. 9 (2009) 287–296.
[35] D. Zhongwei, L. Liying, M. Runyu, Study on the effect of flow maldistribution on the performance of the hollow fiber modules used in membrane distillation, J. Membr. Sci. 215 (2003) 11–23.
[36] H. Fan, Y. Peng, Application of PVDF membranes in desalination and comparison of the VMD and DCMD processes, Chem. Eng. Sci. 79 (2012) 94–102.
[37] K.W. Lawson, D.R. Lloyd, Membrane distillation. I. Module design and performance evaluation using vacuum membrane distillation, J. Membr. Sci 120 (1996) 111–121.
[38] T.D. Dao, J.P. Mericq, S. Laborie, C. Cabassud, A new method for permeability measurement of hydrophobic membranes in Vacuum Membrane Distillation process, Water Res. 47 (2013) 2096–2104.
[39] W. Kast, C.R. Hohenthanner, Mass transfer within the gas-phase of porous media, Int. J. Heat Mass Transfer 43 (2000) 807–823.
[40] R.G. Perry, C.H. Chilton, S.D. Kirkpatrick, Perry's Chemical Engineers Handbook, McGraw Hill Education, New York, NY, 1999, p. 2.125.
[41] N. Zhang, D.J. Chato, J.B. McQuillen, B.J. Motil, D.F. Chao, CFD simulation of pressure drops in liquid acquisition device channel with sub-cooled oxygen, Int. J. Aerospace Mech. Eng. 5 (2011) 203–208.
[42] J.-M. Li, Z.-K. Xu, Z.-M. Liu, W.-F. Yuan, H. Xiang, S.-Y. Wang, Y.-Y. Xu, Microporous polypropylene and polyethylene hollow fiber membranes. Part 3. Experimental studies on membrane distillation for desalination, Desalination 155 (2003) 153–156.
[43] M. Khayet, T. Matsuura, Preparation and characterization of polyvinylidene fluoride membranes for membrane distillation, Ind. Eng. Chem. Res. 40 (2001) 5710–5718.
[44] G. Naidu, Y. Choi, S. Jeong, T.M. Hwang, S. Vigneswaran, Experiments and modeling of a vacuum membrane distillation for high saline water, J. Ind. Eng. Chem. 20 (2014) 2174–2183.
[45] T. Mohammadi, M.A. Safavi, Application of Taguchi method in optimization of desalination by vacuum membrane distillation, Desalination 249 (2009) 83–89.
[46] C.R. Ramakrishnaiah, C. Sadashivaiah, G. Ranganna, Assessment of water quality index for the groundwater in Tumkur Taluk, Karnataka State, India, J. Chem. 6 (2009) 523–530.